Inferences of a Layered Structure from S Wave Spectra Part 1. Theretical Considerations of S Wave Spectrum Method†

By

Tuneto KURITA*

Department of Transportation Engineering, Faculty of Engineering, Kyoto University

and

Takeshi MIKUMO

Disaster Prevention Research Institute, Kyoto University

Abstract

A method is described to infer a layered structure from the amplitude ratio of the vertical to the horizontal component of SV waves together with the phase difference between them, and also from the corresponding relations between SH waves and the horizontal component of SV waves. The behaviors of these frequency-dependent functions for various models with different layer parameters are investigated, and their applicability to inference of the structure is discussed.

It is shown that the S wave spectra will be useful to test the appropriateness of probable models derived from P wave spectra and other information, if good records from deep-focus shocks with appropriate epicentral distances are analyzed.

§ 1. Introduction

In previous papers (KURITA, 1969a, b, 1970), a method was shown to infer a layered structure from the amplitude and phase spectra of long-period P waves, and the crustal and upper mantle structure in some regions of Japan was determined by this method. In the present paper, the corresponding method for the case of S waves is proposed and will be applied to test the appropriateness of the layered models derived from the P wave spectra. Theoretical studies on the crustal response of plane SV and SH waves was made by HASKELL (1960, 1962), and a method to estimate the crustal thickness has been shown by IBRAHIM (1969), using the minima in the amplitude spectrum and the zero phase in the phase spectrum of SH waves, and applied to several stations.

In Part I of this paper, the method is described to infer a layered structure from the amplitude ratio of the vertical to the horizontal component of long-period SV waves together with the phase difference between them, and the corresponding relation between SH waves and the horizontal component of SV waves. Thereafter, the theoretical amplitude ratio and phase difference for SV and SH waves are computed for various models to examine their behavior and applicability to inference of the layered structure.

§ 2. Method of Analysis

On the assumption that the crustal and subcrustal structure is composed of homogeneous isotropic parallel layers, we consider plane SV and SH waves incident at the base of the stratified layers.

The amplitude and phase spectra, $A_{SV(w,u)}(\omega)$ and $P_{SV(w,u)}(\omega)$, of the vertical and horizontal components of the SV waves observed at any station may be written in the forms,

$$A_{SV(w,u)}(\omega)=A_{S\text{-}SV}(\omega)\cdot A_{SC\text{-}SV(w,u)}(\omega)\cdot$$

* Now at Seismological Laboratory, California Institute of Technology, Pasadena, California, 91109.

† Contribution No. 1976, Division of Geological and Planetary Sciences, California Institute of Technology, Pasadena, California 91109.

$$A_{M\text{-}SV}(\omega)\cdot A_{C\text{-}SV(w,u)}(\omega)\cdot A_I(\omega) \quad (1)$$

$$P_{SV(w,u)}(\omega)=P_{S\text{-}SV}(\omega)+P_{SC\text{-}SV(w,u)}(\omega)+P_{M\text{-}SV}(\omega)+P_{C\text{-}SV(w,u)}(\omega)+P_I(\omega) \quad (2)$$

where $A_{S\text{-}SV}(\omega)$, $P_{S\text{-}SV}(\omega)$; $A_{SC\text{-}SV(w,u)}(\omega)$, $P_{SC\text{-}SV(w,u)}(\omega)$; $A_{M\text{-}SV}(\omega)$, $P_{M\text{-}SV}(\omega)$; $A_{C\text{-}SV(w,u)}(\omega)$, $P_{C\text{-}SV(w,u)}(\omega)$; and $A_I(\omega)$, $P_I(\omega)$ are the amplitude and phase responses of the source function, source crust-upper mantle transfer function, mantle transfer function mainly due to anelasticity in the mantle, the crust-upper mantle transfer function at the station, and the instrumental response, respectively. The fourth amplitude and phase responses are associated with the layered structure now considered. From the above relations, we have

$$A_{SVw}(\omega)/A_{SVu}(\omega)=A_{C\text{-}SVw}(\omega)/A_{C\text{-}SVu}(\omega) \quad (3)$$

and

$$P_{SVw}(\omega)-P_{SVu}(\omega)=P_{C\text{-}SVw}(\omega)-P_{C\text{-}SVu}(\omega)+2n\pi \quad (4)$$

(n is an integer), if we assume that the effect of the crust-upper mantle structure around the source can be neglected for deep-focus earthquakes.

For SH (horizontally polarized shear) waves, we have similar relations,

$$A_{SH}(\omega)=A_{S\text{-}SH}(\omega)\cdot A_{SC\text{-}SH}(\omega)\cdot A_{M\text{-}SH}(\omega)\cdot A_{C\text{-}SH}(\omega)\cdot A_I(\omega) \quad (5)$$

$$P_{SH}(\omega)=P_{S\text{-}SH}(\omega)+P_{SC\text{-}SH}(\omega)+P_{M\text{-}SH}(\omega)+P_{C\text{-}SH}(\omega)+P_I(\omega) \quad (6)$$

Each of the source amplitude spectra $A_{S\text{-}SV}(\omega)$ and $A_{S\text{-}SH}(\omega)$ includes a frequency-dependent part and a spatial coefficient depending on the source mechanism. Since the former part is common to both types of waves, $A_{S\text{-}SH}(\omega)/A_{S\text{-}SV}(\omega)$ may be reduced to a frequency-independent constant, and generally connected with the polarization angle ε (STAUDER, 1960; NUTTLI, 1964). The source phases of SV and SH waves may be regarded as the same. We may also assume that the effects of anelasticity on the passing SV and SH waves are the same. Therefore, if we take the amplitude ratio and phase difference between SH waves and the horizontal component of SV waves, using eqs. (1), (5), (2) and (6), the following two relations hold:

$$A_{SH}(\omega)/A_{SVu}(\omega)=(A_{S\text{-}SH}(\omega)/A_{S\text{-}SV}(\omega))\cdot(A_{C\text{-}SH}(\omega)/A_{C\text{-}SVu}(\omega))=\tan\varepsilon\cdot A_{C\text{-}SH}(\omega)/A_{C\text{-}SVu}(\omega) \quad (7)$$

$$P_{SH}(\omega)-P_{SVu}(\omega)=P_{C\text{-}SH}(\omega)-P_{C\text{-}SVw}(\omega)+2n\pi \quad (8)$$

Thus we obtain two pairs of expressions independent on the spectrum of incident S waves, and these may be used to infer a layered structure beneath the station. Eqs. (7) and (8) can also be derived from equation 7 of NUTTLI (1964).

The left-hand sides of eqs. (3), (4), (7) and (8) can be obtained in the following way from the Fourier analysis of long-period S waves recorded on three component seismograms. The horizontal component of SV waves, $f_{SVu}(t)$, and SH waves, $f_{SH}(t)$, are derived from the two horizontal components, the NS record $f_N(t)$ and the EW record $f_E(t)$, simply by the rotation of axes,

$$f_{SVu}(t)=f_N(t)\cos\phi+f_E(t)\sin\phi$$
$$f_{SH}(t)=f_E(t)\sin\phi-f_E(t)\cos\phi$$

where ϕ is the azimuth measured from the north seen from the station to the event. $f_{SVu}(t)$ is taken positive away from the epicenter, and $f_{SH}(t)$ is taken positive for clockwise motion as seen from the epicenter. The technique employed in obtaining Fourier transforms of the resolved records is similar to that used for P waves (KURITA, 1969a).

The right-hand sides of the corresponding expressions, which are termed hereafter as theoretical functions, can be calculated by using the Haskell-Thomson matrix method (HASKELL, 1960, 1962) for variously assumed models and for the angle of incidence at the base of the strata, i_{ns}. This angle is related to the horizontal phase velocity c with $c=\beta_n/\sin i_{ns}$ (β_n being the shear velocity just under the strata), and will be specified by the epicentral distance and depth of the earthquake analyzed and the velocity distribution in the mantle. Fig. 1 (a) and (b) give two examples of the transfer functions of SV and SH waves,

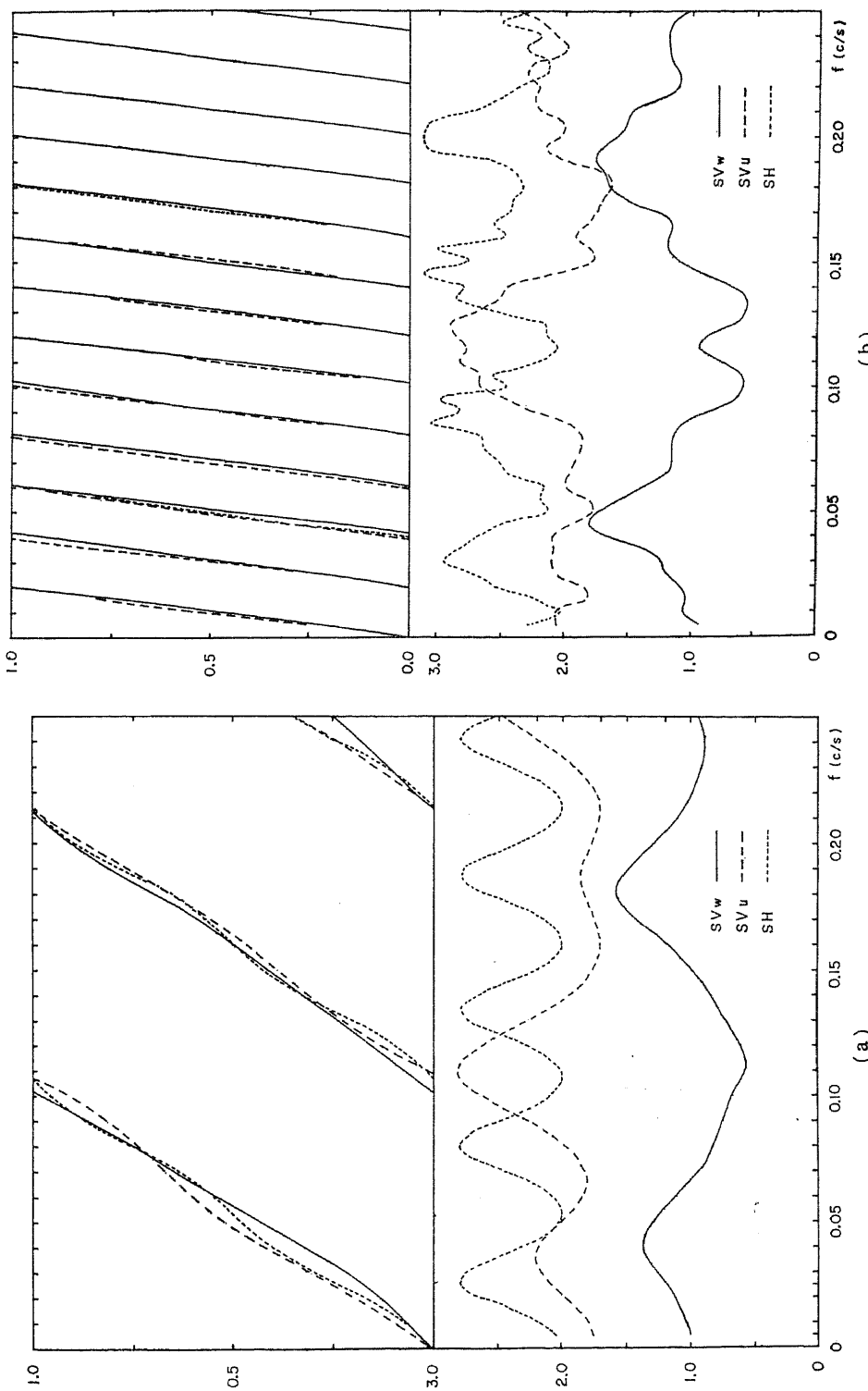

Fig. 1. Crustal response of SV and SH waves for an incident angle of 30°. Upper; phase delay in parts of circle, lower; amplitude, (a) Unilayered model of Haskell, (b) modified Anderson-Kovach model.

$A_{C\text{-}SV_W}(\omega)$, $A_{C\text{-}SV_U}(\omega)$, $A_{C\text{-}SH}(\omega)$, $P_{C\text{-}SV_W}(\omega)$, $P_{C\text{-}SV_U}(\omega)$, and $P_{C\text{-}SH}(\omega)$, for the Unilayered model of HASKELL (1960) and a model modified from those of BRUNE and DORMAN (1963) and ANDERSON and KOVACH (1969). The phase responses shown in the upper part of the figures are indicated as delay in parts of circle. In order to determine the layered structure from comparison between the observations of body waves and the theoretical functions, there could be an inversion fitting technique of using the partial derivatives of the transfer functions with respect to the layer parameters as in the case of surface-wave phase velocities (ANDERSON, 1964). FERNANDEZ (1965) showed, however, that for the transfer function the inversion process based on the assumption that the partial derivatives remain constant for reasonable changes of the layer parameters is not possible.

Therefore, an alternative to be taken is to compute the theoretical functions by assuming various layer parameters and to compare with the observational functions. If the both functions agree to a certain extent, the model may be an approximation to the structure beneath the station.

§ 3. Behavior of Theoretical Functions for SV Waves

In this section, the behaviors of the theoretical amplitude ratio and the phase difference for SV waves are discussed for the models shown in Tables 1 and 2. They include all the models for which the corresponding theoretical functions for P waves have been tested (KURITA, 1969a, 1970). The discussion is confined to the frequency range between 0 and 0.2 cps, since for higher frequencies local geological structure gives serious effects on the wave spectrum.

Fig. 2 illustrates general features of the theoretical functions for the upper four models in Table 1, in the case of an incident angle of 30°. The curves for model 6EJ are similar with those for model 6E, as was the case of P waves, probably due to the layer parameters simply reduced by 5% from those of the latter model. Similarity of these curves with those for the Unilayered model, at lower frequencies, may come from the same total thickness of the strata. The curves for both the amplitude ratio and the phase difference have only one or two peaks, while there are generally three peaks for the curves of P waves in this frequency range. The amplitude ratio ranges from 0 to about 1.0, varying very smoothly with frequency. These are common features in the theoretical curves of SV waves for most of the models mentioned here.

The general tendency described above does not change greatly with variations in incident angle within the range that $c>\alpha_n$, where α_n is the compressional velocity under the strata. However, for incident angles such that c approaches α_n, variation in the amplitude ratio with frequency becomes rather large, and for $c<\alpha_n$ it is erratic and the phase difference is always either plus or minus 90° (HASKELL, 1962). Fortunately, the teleseismic S waves with which we are primarily concerned are incident at angles such that $c>\alpha_n$. Some examples of the theoretical curves of SV waves for the Unilayered model are given in Fig. 3, for incident angles from 33° to 38°. It is to be noted that the amplitude ratio curve shows large variation with a slight change of incident angles over this range, while the phase difference curves are similar for angles less than 36° (for i_n=35° and 36°, c=8.02 and 7.83 km/sec respectively, while α_n=7.96 km/sec). These features are not recognized for P waves. It is clear from Haskell's calculations (1962) and the above considerations that the seismograms with incident angles such that $c<\alpha_n$ cannot be used to infer the layered structure from SV waves. Referring also to another example shown in Figure 3 in KURITA (1970), it might be possible to superpose the observational phase differences from a number of shocks with a considerable range of epicentral distances, although the peak positions for SV waves are more sensitive to the change of incident angles even for the case of $c>\alpha_n$ than for P waves.

In the following, various effects on the theoretical functions are examined, taking an incident angle of 30° as an example.

(*a*) *Effect due to total crustal thickness*

Theoretical curves for the Unilayered model with various crustal thicknesses are compared in Fig. 4. The thickness is taken from 27 to 57 km with an increase of every 10 km. The peak positions shift to lower frequencies as the crust becomes thicker, while the peak amplitudes are preserved. For multilayered models as well as for the Unilayered one, the position of the lowest-frequency peak generally depends on the depth to the lowest sharp discontinuity. This is the same as in the case of P waves.

(*b*) *Effect due to gradual change of layer parameters*

The effects of the existence of a transitional layer at the layer interface are next examined. The theoretical curves shown in Fig. 5 are for the case in which all layer parameters vary linearly with depth between 5 km above and below the boundary. The differences between the case and the Unilayered model are too small to be detected from observations, as in the case of P waves.

(*c*) *Effect due to a thin surface layer*

Thoeretical curves for the Unilayered model

Table 1. List of layered models (1).

Layered Model	α (km/sec)	β (km/sec)	ρ (g/cm^3)	H (km)
Unilayered	6.28	3.63	2.87	37.0
Haskell (1960)	7.96	4.60	3.37	—
Santa Monica-San Francisco	6.10	3.38	2.85	27.0
Healy (1963)	8.20	4.54	3.40	—
6EJ (Japan)	5.70	3.33	2.78	22.0
Aki (1961)	6.33	3.59	3.00	15.0
	7.52	4.35	3.33	—
6E	6.03	3.53	2.78	22.0
Press (1960)	6.70	3.80	3.00	15.0
	7.96	4.60	3.37	—
6EG (Low-velocity Layer)	6.03	3.53	2.78	22.0
Press (1960)	6.70	3.80	3.00	15.0
	7.96	4.60	3.37	13.0
	7.85	4.50	3.39	25.0
	7.85	4.41	3.42	50.0
	8.00	4.41	3.45	75.0
	8.20	4.50	3.47	50.0
	8.40	4.60	3.50	—
Modified A-K	5.64	3.47	2.70	6.0
Brune and Dorman (1963)	6.15	3.64	2.80	10.0
Anderson and Kovach (1969)	6.60	3.85	2.85	19.0
	8.12	4.75	3.32	35.0
	7.93	4.38	3.25	40.0
	7.68	4.20	3.18	80.0
	8.02	4.45	3.26	20.0
	8.32	4.45	3.42	30.0
	8.40	4.60	3.50	—

Table 2. List of layered models (2).

Layered Model	α (km/sec)	β (km/sec)	ρ (g/cm^3)	H (km)	Q_α	Q_β
Unilayered model—U0	6.28	3.63	2.87	37.0	∞	∞
Haskell (1960)	7.96	4.60	3.37	—	∞	∞
Unilayered model with surface low-velocity layer—US1 (US2)	5.10	2.95	2.60	1.0 (3.0)		
	6.28	3.63	2.87	36.0 (34.0)		
	7.96	4.60	3.37	—		
Unilayered model with surface low-velocity layer—US3 (US4)	3.00	1.73	2.00	1.0 (3.0)		
	6.28	3.63	2.87	36.0 (34.0)		
	7.96	4.60	3.37	—		
Dissipative unilayered model—DU0	6.28	3.63	2.87	37.0	500	200
	7.96	4.60	3.37	—	100	40
Dissipative unilayered model—DU1	6.28	3.63	2.87	37.0	500	200
	7.96	4.60	3.37	—	∞	∞
Unlaminated model—UL0 Aki (1968)	5.98	3.45	2.76	20.0		
	6.78	3.81	3.00	10.0		
	8.10	4.70	3.30	—		
Unlaminated model with single soft layer—UL1 (UL2)	5.98	3.45	2.76	20.0		
	6.78	3.81	3.00	10.0		
	7.50	2.70 (1.10)	3.20	1.0		
	8.10	4.70	3.30	—		
Laminated mantle model with soft layers—L1 (L2)	5.98	3.45	2.76	20.0		
	6.78	3.81	3.00	10.0		
	7.50	2.70 (1.10)	3.20	0.2		
	8.10	4.70	3.30	10.0		
	7.50	2.70 (1.10)	3.20	0.2		
	8.10	4.70	3.30	10.0		
	7.50	2.70 (1.10)	3.20	0.2		
	8.10	4.70	3.30	10.0		
	7.50	2.70 (1.10)	3.20	0.2		
	8.10	4.70 (1.10)	3.30	10.0		
	7.50	2.70	3.20	0.2		
	8.10	4.70	3.30	—		

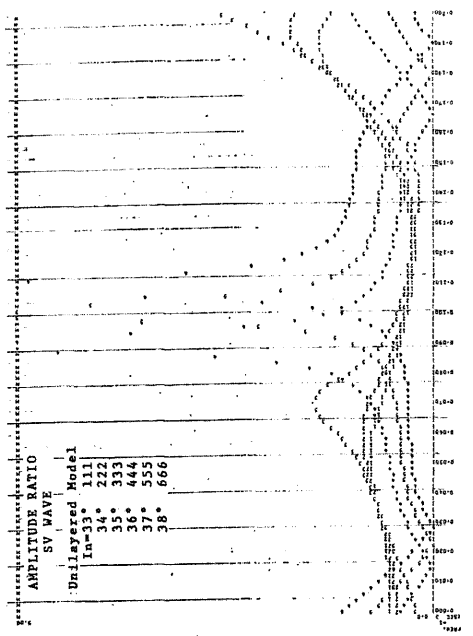

Fig. 2. Theoretical amplitude ratio (upper) and phase difference (lower) for the four models in Table 1.

Fig. 3. Theoretical amplitude ratio (upper) and phase difference (lower) for Unilayered model in the case of incident angles from 33° to 38°.

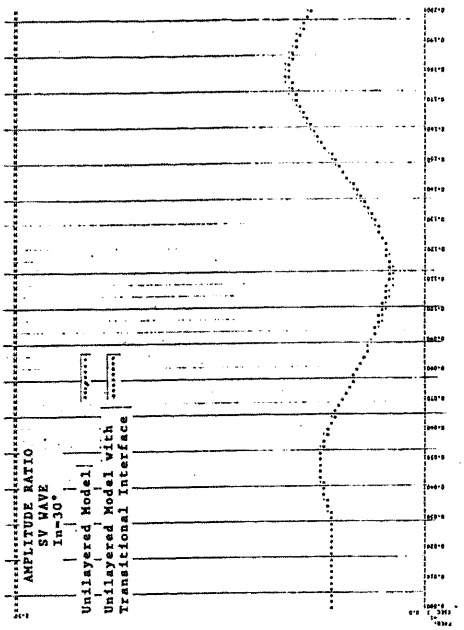

Fig. 4. Theoretical amplitude ratio (upper) and phase difference (lower) for Unilayered models with crustal thicknesses from 27 to 57 km.

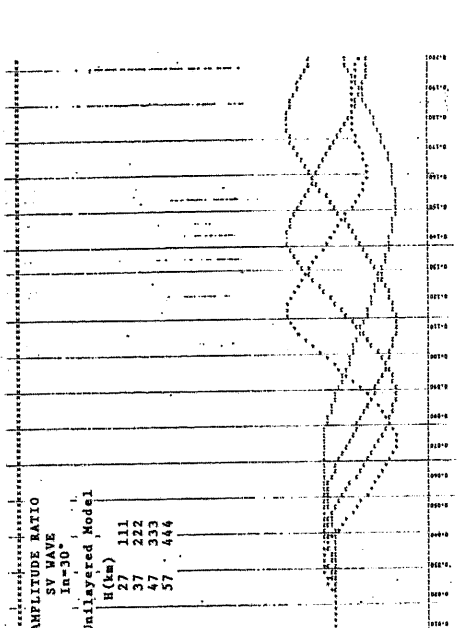

Fig. 5. Theoretical amplitude ratio (upper) and phase difference (lower) for Unilayered model and a model with a transitional layer at the crust-mantle boundary.

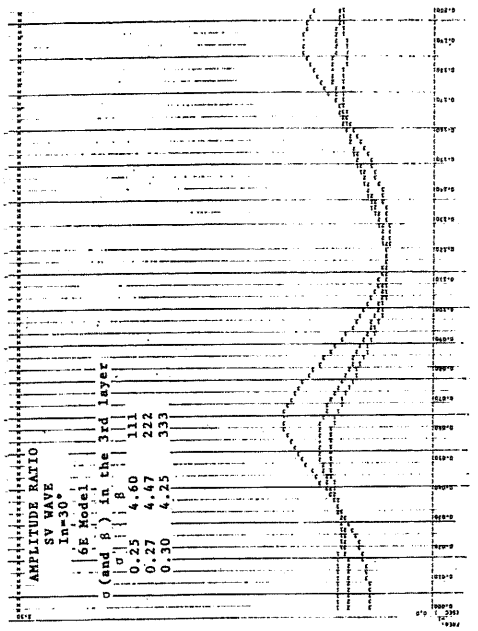

Fig. 7. Theoretical amplitude ratio (upper) and phase difference (lower) for model 6E with Poisson's ratio of 0.25 and modified 6E models with Poisson's ratios of 0.27 and 0.30 in the mantle; SV waves.

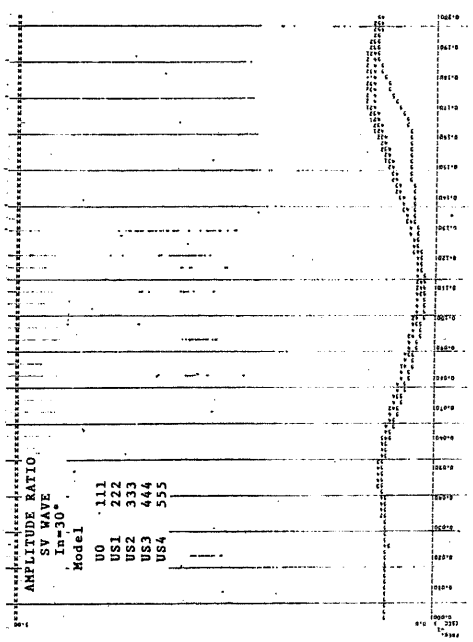

Fig. 6. Theoretical amplitude ratio (upper) and phase difference (lower) for Unilayered models with a thin surface layer; SV waves.

overlain by such a thin surface layer as indicated in Table 2 are given in Fig. 6 for SV waves. It may be inferred from a comparison among these curves that the effects of the surface layer become noticeable in higher frequencies if its thickness with a shear velocity lower than about 2 km/sec is over 3 km, and seems to be rather serious for SV waves than for P waves.

(*d*) *Effect due to high Poisson's ratio in the upper mantle*

Fig. 7 shows a comparison among the theoretical curves for SV waves of model 6E with Poisson's ratio of 0.25, and its modifications with the ratios of 0.27 and 0.30 in the upper mantle. The comparison indicates that for P waves an increase of the ratio from 0.25 to 0.30 does not give much effects on the peak position, but for SV waves it has considerable effects on the curves.

(*e*) *Effect due to the low velocity layer*

Fig. 8 depicts the theoretical curves for a model including the low velocity layer in the upper mantle, 6EG, in comparison with those of a model without that layer, 6E. In the former model there clearly appears short-period undulations particularly in the phase difference curves. The undulations in the case of P waves were not so remarkable as for SV waves (KURITA, 1969a). There is a possibility, therefore, that the existence of the low velocity layer in the upper mantle could be confirmed from observed S wave spectra.

(*f*) *Effect due to anisotropy or laminations*

It has been stated (BACKUS, 1961; AKI, 1968) that for low frequencies a transversely isotropic model can be approximated by laminated mantle models with alternating layers of hard and soft materials. The difference between these models in the transfer function of body waves over the frequency range under consideration will be examined in Part 3. Fig. 9 shows comparison between laminated mantle models (L1 and L2) and unlaminated models (UL0, UL1 and UL2) shown in Table 2, which are the same as those in a previous paper (KURITA, 1970). It appears from these figures that it would be difficult to discriminate models UL1 and L1, in which a shear velocity in the soft layer interleaved between the crust and the uppermost mantle is 2.70 km/sec, from the model without the layer (UL0). However, if the shear velocity is as low as 1.10 km/sec, the theoretical curves for models UL2 and L2 show some departure from those for UL0. For models with the velocity between 1.10 and 2.70 km/sec, the curves fall between the two cases. Moreover, the general features of the curves are not lost, even if the thickness of the soft layer or their interleaved depths change slightly. From the above considerations, it follows that the existence of interleaved soft layers could be identified only when the shear velocity is of the order of 1 km/sec.

(*g*) *Effect due to dissipation*

We can estimate the effect of dissipation on the body wave transfer characteristics by introducing complex velocities as HASKELL (1953) suggested. CLOWES and KANASEWICH (1970) computed the transfer function for vertical incidence of P waves in dissipative media. Following PRESS and HEALY (1957) we introduce dissipation by transforming from real to complex velocities. Denoting by $\bar{\alpha}_m$ and $\bar{\beta}_m$ the complex compressional and shear velocities in the mth layer, and by $\bar{c}$ the complex phase velocity, for large Q values we may set with a good approximation in the matrix formulation in deriving the transfer function

$$\bar{\alpha}_m=\alpha_m\left(1+\frac{i}{2Q_{\alpha m}}\right) \qquad (m=1, 2, \ldots, n)$$

$$\bar{\beta}_m=\beta_m\left(1+\frac{i}{2Q_{\beta m}}\right) \qquad (m=1, 2, \ldots, n)$$

$$\bar{c}=c\left(1+\frac{i}{2Q_{\beta n}}\right)$$

where $c=\beta_n/\sin i_{ns}$. The theoretical curves for dissipative and non-dissipative models are compared in Fig. 10, in the case of incident angles of 30° and 40°. In the dissipative models, the layer parameters are taken as the same as for the Unilayered model, and Q values are tentatively given as in Table 2. It can be seen that for an incident angle of 30°, both the amplitude and phase difference

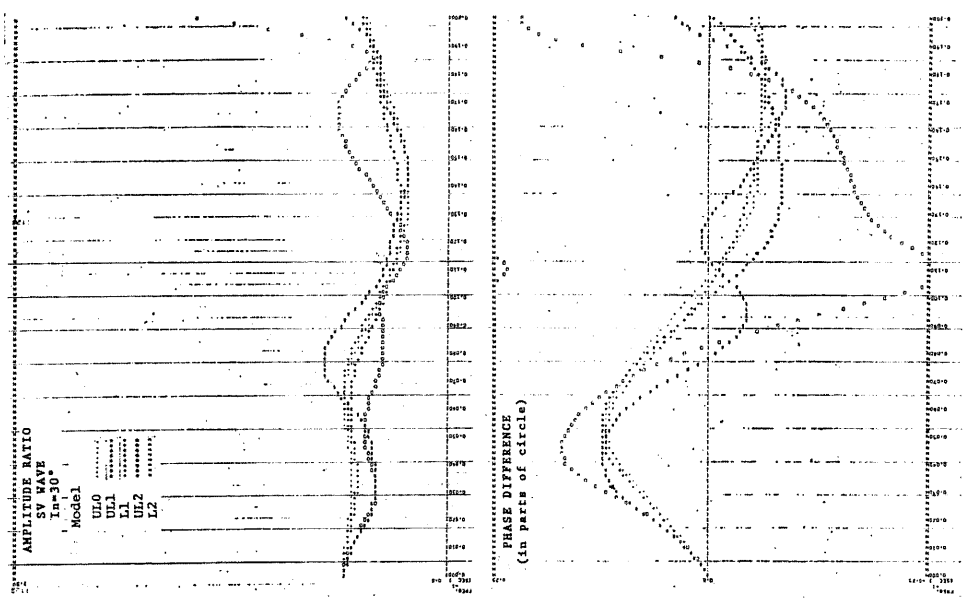

Fig. 9. Theoretical amplitude ratio (upper) and phase difference (lower) for laminated mantle medels and unlaminated models with soft layers.

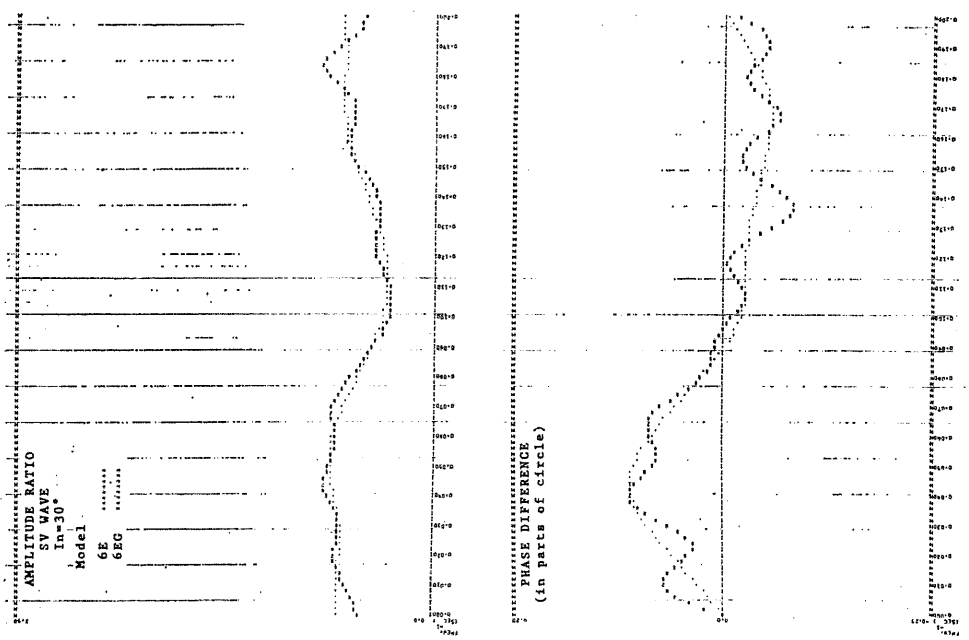

Fig. 8. Theoretical amplitude ratio (upper) and phase difference (lower) for model 6EG with the low velocity layer in the upper mantle and model 6E without it.

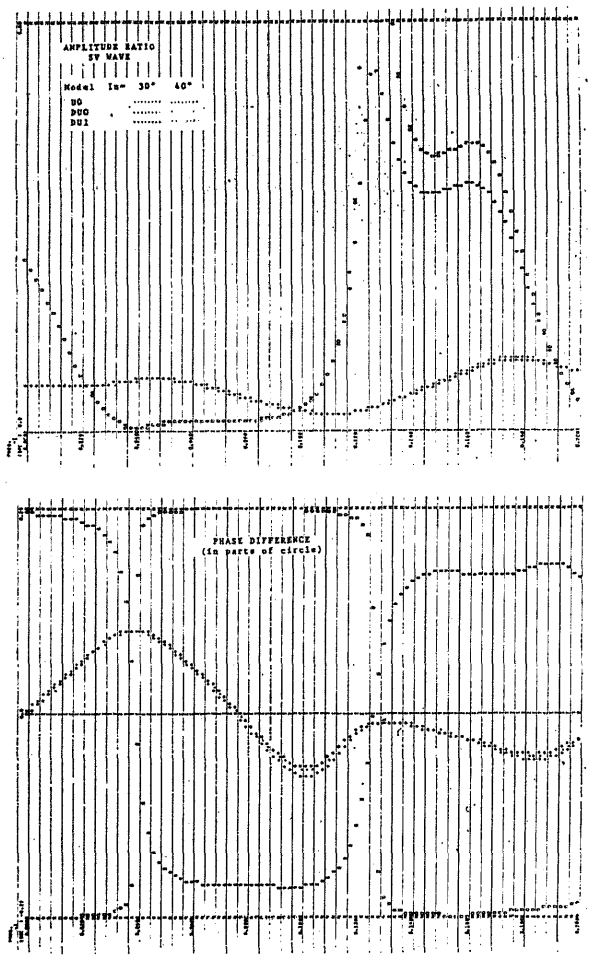

Fig. 10. Theoretical amplitude ratio (upper) and phase difference (lower) for dissipative and non-dissipative unilayered models.

curves for the dissipative models do not show a marked difference from those of the non-dissipative model. For the angle of 40° for which c (=7.16 km/sec) is smaller than α_n (=7.96 km/sec), the difference becomes apparently remarkable particularly in the phase difference curve, as Q values become smaller. More detailed discussions on the effects of dissipation will be made elsewhere.

ISHII and ELLIS (1970) calculated the amplitude response for single layered models with an inclined interface of various dip angles, for the incidence of P and SV waves from various directions. Although the effect of dipping interface is not large for P waves over the frequency range now in consideration, this cannot necessarily be ignored for SV waves, as shown in Fig. 3-7 and 3-9 in their paper.

§ 4. Behavior of Theoretical Functions for SH Waves

In this section, the behaviors of theoretical functions including SH waves are discussed, since SH waves contain independent information on the layered structure to that from SV

waves. Although an attempt has been made by IBRAHIM (1969) to use the spectra of SH waves to estimate the crustal thickness, the observed spectra involve various effects as expressed in eqs. (5) and (6). To extract only the structure information from observations, we take the amplitude ratio and phase difference between SH waves and the horizontal component of SV waves as given in eqs. (7) and (8).

The discussion here is made for the same layered models as in the case of SV waves for the sake of comparison, within the frequency range between 0.005 to 0.25 cps. It has been shown (HASKELL, 1960) that the amplitude and phase responses of SH waves, as shown in Figs. 1-(a) and (b) as examples, show similar shape of undulations even for large incident angles such that $c<\alpha_n$. For this range of incident angles, particularly that for $\alpha_1<c<\alpha_n$, however, the spectra of the horizontal component of SV waves show rapid fluctuations with frequency (HASKELL, 1962), so that the theoretical functions composed of SH and SV waves also vary too rapidly to compare with observations. For this reason, we confine ourselves in this section to the case for which $c>\alpha_n$.

Theoretical considerations for the cases corresponding to (b) and (g) in the foregoing section have been omitted, since the effects in the cases have proved insignificant.

Fig. 11 shows the amplitude ratios and phase differences between SH waves and the horizontal component of SV waves for the unilayered model, models 6E and 6EG, in the case of an incident angle of 30° with $\tan\varepsilon=1$. The general features particularly of peak positions for frequencies lower than 0.2 cps do not differ greatly for the models, although they have somewhat different layer compositions. This is attributable to the same crustal thickness.

(a) Fig. 12 gives an illustration of the theoretical functions for the unilayered model with varying thickness. We see that the lowest and the second-lowest frequency peaks move to the lower frequency side, or that the number of peaks for frequencies lower than 0.2 cps increases from three to six, as the crustal thickness changes from 27 to 57 km. This situation contrasts sharply with one or two peaks in the corresponding functions for SV waves as described in the preceding section, and will make it with higher precision to estimate the crustal thickness from observations.

(b) The effects of the existence of a thin surface layer over the unilayered model are next examined. The theoretical curves for three cases are given in Fig. 13. The curves for models US1 and US3 are not shown here because of their slight departure from that for US0. It is noticed that if the thickness with a shear velocity lower than 2 km/sec exceeds the order of 3 km, the effects become serious for frequencies higher than 0.15 cps.

(c) Fig. 14 shows the theoretical functions for model 6E with varying Poisson's ratio from 0.25 to 0.29 in the upper mantle. It is seen that the change in the ratio over this range does not give much effects on the peak positions.

(d) In Fig. 15 are illustrated the theoretical curves for three models involving a low velocity layer in the upper mantle. A comparison between the curves for model 6EG with the layer and model 6E without it does not indicate large effects of the low velocity layer, as seen from Fig. 11. However, three models 6EG, A-K (a model modified from BRUNE and DORMAN (1963) and ANDERSON and KOVACH (1969)), and A-K′ (a more simplified model of A-K, by replacing the 5-, 6- and 7-th layers by the 4-th layer with a thickness of 140 km) show characteristic differences in the curves. We notice that both the amplitude ratio and the phase difference are more superposed by short-period fluctuations as the shear velocity contrast between the low velocity layer and the upper and lower media becomes pronounced. This property would be useful for identification of the low velocity layer.

(e) The behaviors of the theoretical functions are tested for the effects of interleaved soft layers. Fig. 16 gives two unlaminated models UL1 and UL2 and a laminated model L2, together with their original model. Model

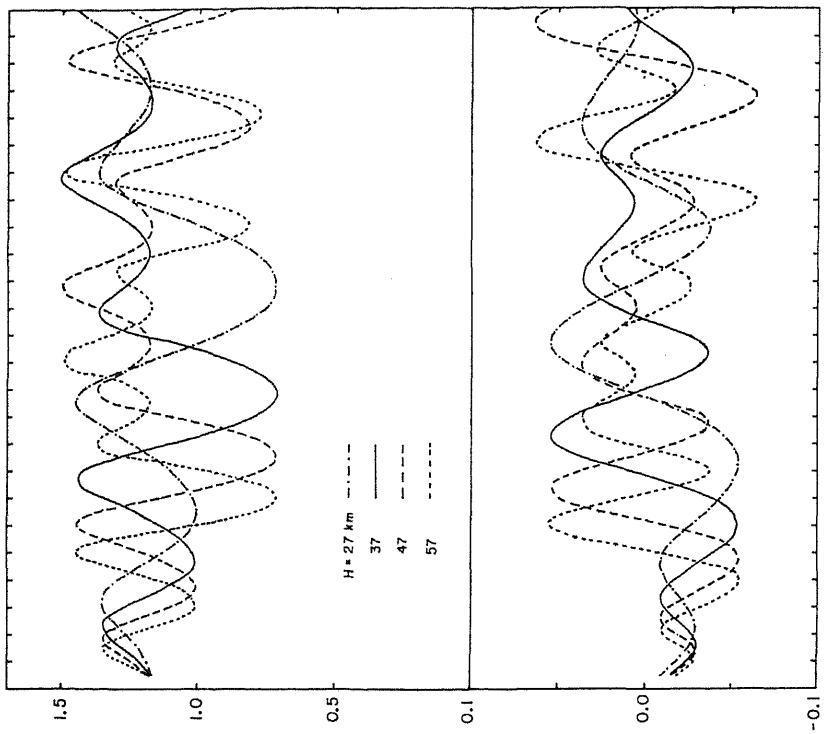

Fig. 12. Theoretical amplitude ratio (upper) and phase difference (lower) between SH and SV waves for Unilayered models with a crustal thickness from 27 to 57 km.

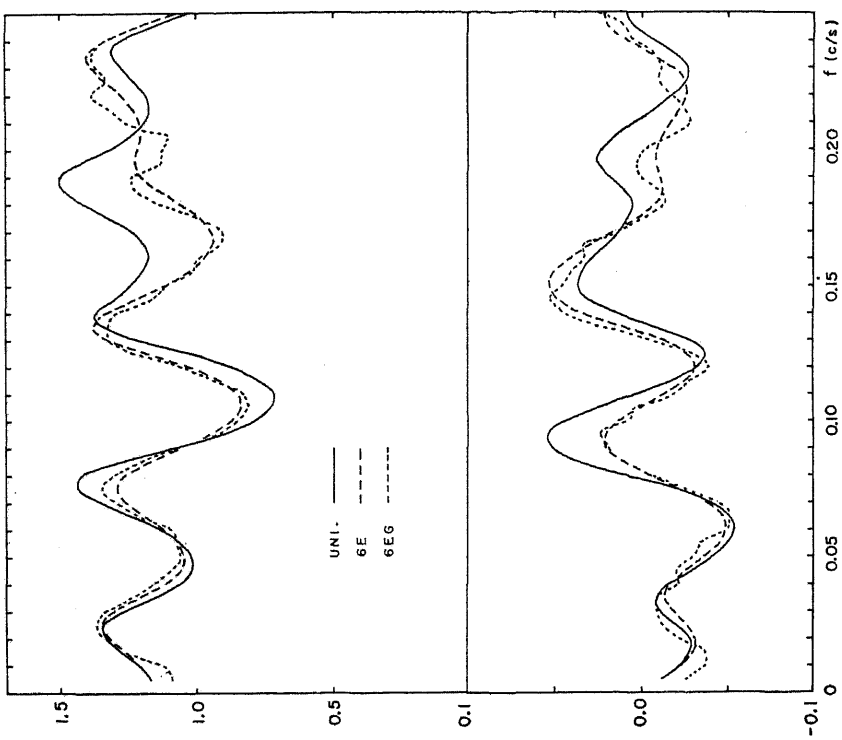

Fig. 11. Theoretical amplitude ratio (upper) and phase difference (lower) between SH and SV waves for the three models in Table 1.

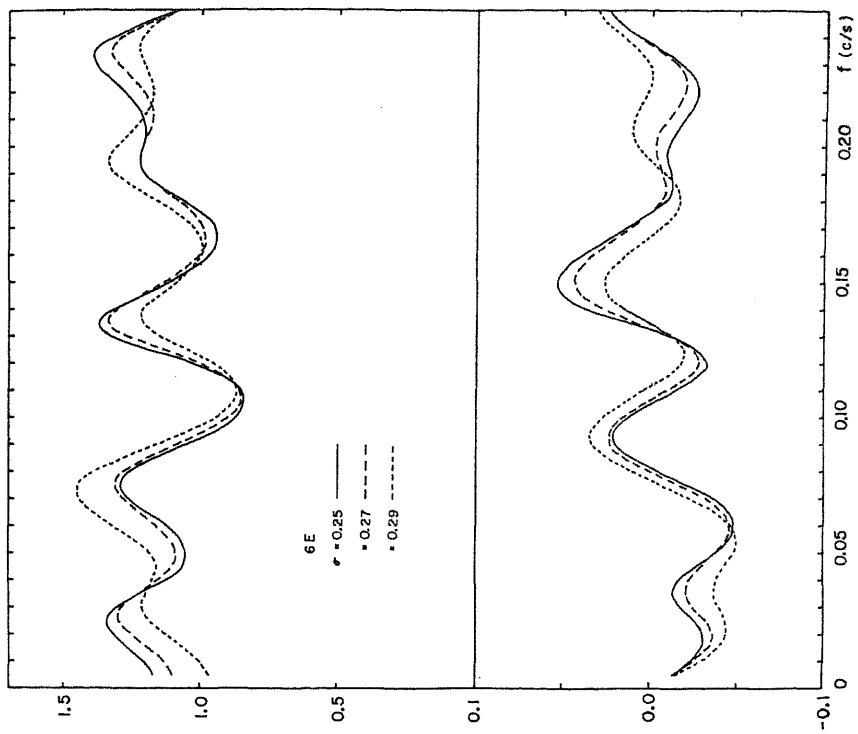

Fig. 14. Theoretical amplitude ratio (upper) and phase difference (lower) between SH waves and SV waves for model 6E with varying Poisson's ratio from 0.25 to 0.29.

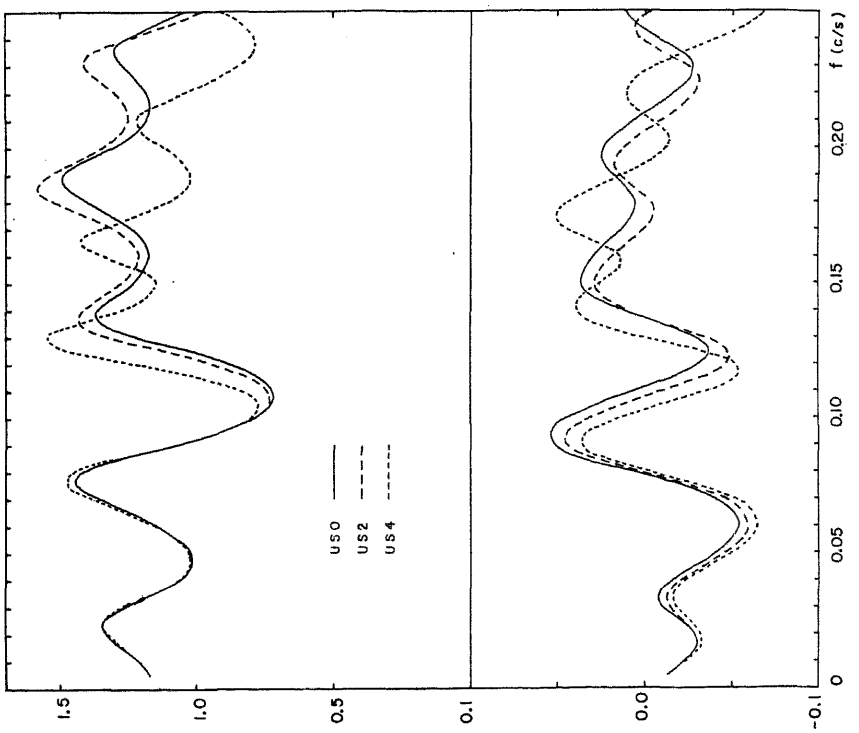

Fig. 13. Theoretical amplitude ratio (upper) and phase difference (lower) between SH and SV waves for the unilayered models with a thin surface layer.

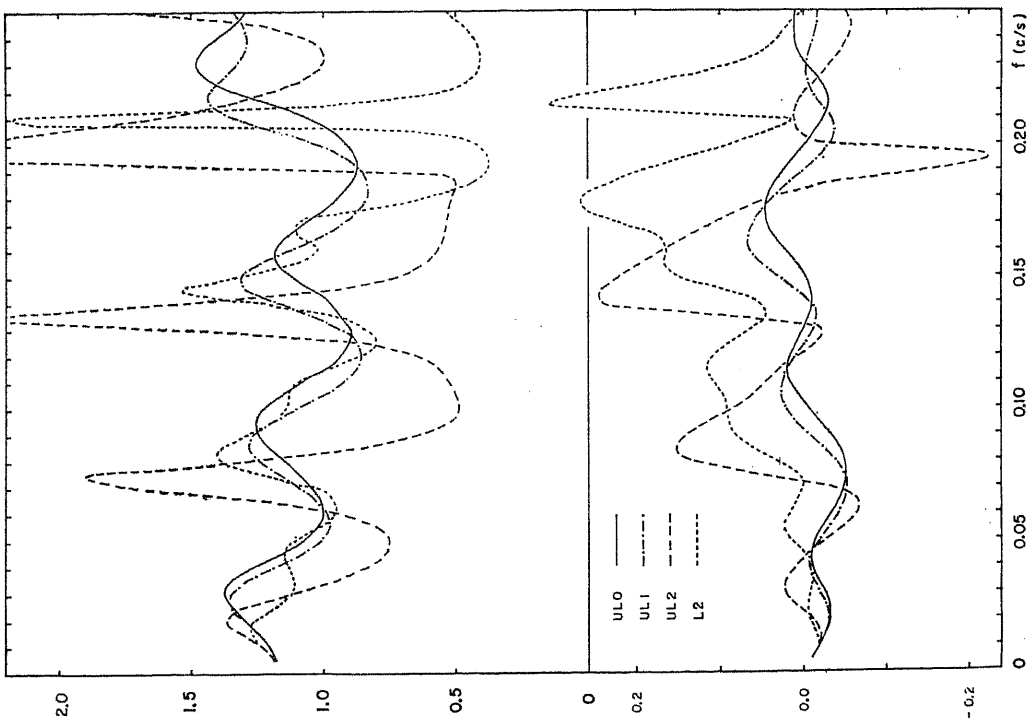

Fig. 16. Theoretical amplitude ratio (upper) and phase difference (lower) between SH and SV waves for laminated mantle models and unlaminated models with soft layers.

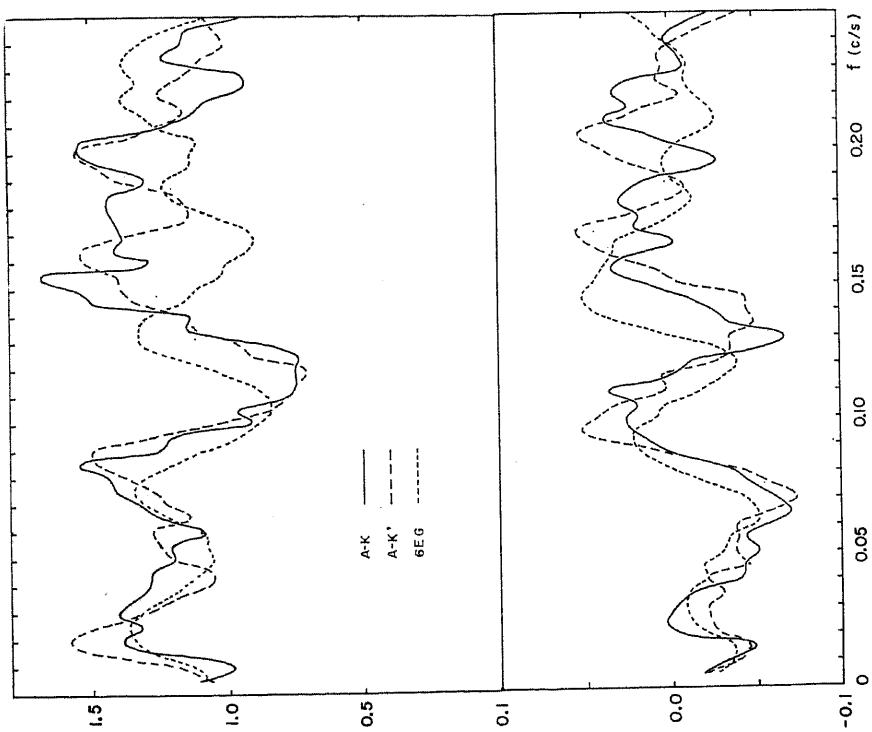

Fig. 15. Theoretical amplitude ratio (upper) and phase difference (lower) between SH and SV waves for three models including the low velocity layer.

L1, a laminated model with a shear velocity of 2.7 km/sec, does not yield much difference from the curves for UL0, as in the case of UL1. However, it is noticed that if there are interleaved layers with a total of 1 km thickness having a shear velocity as low as 1.0 km/sec, the theoretical curves lose their original features. It would therefore be possible to infer from observations whether this kind of layers exist in the upper mantle.

§ 5. Summary

We have examined theoretically the behaviors of the frequency-dependent amplitude ratio and phase difference between the vertical to the horizontal component of SV waves, and between SH waves and the horizontal component of SV waves, for variations of layer compositions. For incident angles such that $c<\alpha_n$, the amplitude ratios are too sensitive to variations in the incident angle, while the phase differences are kept constant to be $\pm 90°$, as seen in Section 3. The characteristics of the theoretical functions in the case of $c>\alpha_n$ may be summarized as follows:

i) The theoretical functions for SV waves show gentle variations with frequency, having only one or two peaks, whereas those including SH waves have more peaks within the frequency range under consideration as in the case of P waves. ii) The latter functions are more sensitive than the former to variations in the crustal thickness. iii) Both functions are rather sensitive for S wave velocities in the upper mantle particularly for the case including a low velocity layer. iv) On the other hand, the theoretical functions for both SV and SH waves are not sensitive to the existence of transitional layers and thin surface layers and to dissipation in the medium, within the frequency range from 0 to 0.2 cps, as have been shown for P waves.

On the observational side, it is necessary to satisfy the conditions that direct S waves are not contaminated by preceding and later phases and have incident angles such that $c>\alpha_n$. These conditions may be satisfied if we select S wave records from deep-focus earthquakes with epicentral distances between 40° and 60°.

It may be concluded that the amplitude and phase spectra of S waves will be useful to infer the crustal and upper mantle structure by testing the appropriateness of a number of models derived from P wave spectra and some other information and selecting probable models among them.

Experimental studies along this line will be made in Part 2 (KURITA, 1971) and Part 3 (MIKUMO and KUKITA, 1971).

Acknowledgments

The computations involved were carried out at Kyoto University Data Processing Center and partly at the Computing Center of California Institute of Technology.

References

Aki, K., Crustal structure in Japan from the phase velocity of Rayleigh waves, Part 1. Use of the network of seismological stations operated by the Japan Meteorological Agency, *Bull. Earthq. Res. Inst.*, **39**, 255-283, 1961.

Aki, K., Seismological evidence for the existence of soft thin layers in the upper mantle under Japan, *J. Geophys. Res.*, **73**, 585-594, 1968.

Anderson, D. L., Universal dispersion tables 1, Love waves across oceans and continents on a spherical earth, *Bull. Seism. Soc. Amer.*, **54**, 681-726, 1964.

Anderson, D. L., and R. L. Kovach, Universal dispersion tables III, Free oscillation variational parameters, *Bull. Seism. Soc. Am.*, **59**, 1667-1693, 1969.

Backus, G. E., Long-wave elastic anisotropy produced by horizontal layering, *J. Geophys. Res.*, **67**, 4427-4440, 1962.

Brune, J. N. and J. Dorman, Seismic waves and earth structure in the Canadian shield, *Bull. Seism. Soc. Amer.*, **53**, 167-210, 1963.

Clowes, R. M., and E. R. Kanasewich, Seismic attenuation and the nature of reflecting horizons within the crust, *J. Geophys. Res.*, **75**, 6693-6705, 1970.

Fernandez, L. M., The determination of crustal thickness from the spectrum of P waves, Saint Louis University, St. Louis, Missouri, Scientific Report No. 13, 1965.

Haskell, N. A., The dispersion of surface waves on multilayered media, *Bull. Seism. Soc. Amer.*, **43**, 17-34, 1953.

Haskell, N. A., Crustal reflection of plane SH waves,

J. Geophys. Res., **65**, 4147-4160, 1960.

Haskell, N. A., Crustal reflection of plane P and SV waves, *J. Geophys. Res.*, **67**, 4751-4767, 1962.

Healy, J. H., Crustal structure along the coast of California from seismic refraction measurements, *J. Geophys. Res.*, **68**, 5777-5787, 1963.

Ibrahim, A. K., Determination of crustal thickness from spectral behavior of SH waves, *Bull. Seism. Soc. Amer.*, **59**, 1247-1258, 1969.

Ishii, H., and R. M. Ellis, Multiple reflection of plane P and SV waves by a dipping layer, *Geophys. J. R. Astr. Soc.*, **20**, 11-30, 1970.

Kurita, T., Crustal and upper mantle structure in Japan from amplitude and phase spectra of long-period P-waves, Part 1. Central mountain area, *J. Phys. Earth*, **17**, 13-41, 1969a.

Kurita, T., Crustal and upper mantle structure in Japan from amplitude and phase spectra of long-period P-waves, Part 2. Kanto plain, Special Contributions, Geophys. Inst., Kyoto Univ., No. 9, 137-166, 1969b.

Kurita, T., Crustal and upper mantle structure in Japan from amplitude and phase spectra of long-period P waves, Part 3. Chugoku region, *J. Phys. Earth*, **18**, 1-26, 1970.

Kurita, T., Inferences of a layered structure from S wave spectra, Part 2. Study of the structure in selected regions of Japan, *J. Phys. Earth*, **19**, (in press).

Mikumo, T. and T. Kurita, Inferences of a layered structure from S wave spectra, Part 3, SH and SV waves and some related problems, *J. Phys. Earth*, **19**, (in press).

Nuttli, O. W., The determination of S-wave polarization angles for an earth model with crustal layering, *Bull. Seism. Soc. Am.*, **54**, 1429-1440, 1964.

Press, F., Crustal structure in the California-Nevada region, *J. Geophys. Res.*, **65**, 1039-1051, 1960.

Press, F., and J. Healy, Absorption of Rayleigh waves in low-loss media, *J. Appl. Phys.*, **28**, 1323-1325, 1957.

Stauder, W., An application of S waves to focal mechanism studies, Publ. Dominion Obs., Ottawa, **24**, 343-354, 1960.

(Received March 22, 1971)